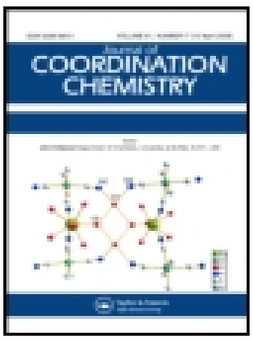

Journal of Coordination Chemistry

ISSN: 0095-8972 (Print) 1029-0389 (Online) Journal homepage: http://www.tandfonline.com/loi/gcoo20

Alkyl chain length effect on construction of copper(II) complexes with tridentate Schiff base ligand and DNA interaction

Rasoul Vafazadeh, Fariba Jafari, Mohammad Mehdi Heidari & Anthony C. Willis

To cite this article: Rasoul Vafazadeh, Fariba Jafari, Mohammad Mehdi Heidari & Anthony C. Willis (2016): Alkyl chain length effect on construction of copper(II) complexes with tridentate Schiff base ligand and DNA interaction, Journal of Coordination Chemistry, DOI: 10.1080/00958972.2016.1163547

To link to this article: http://dx.doi.org/10.1080/00958972.2016.1163547

Publisher: Taylor & Francis

Journal: *Journal of Coordination Chemistry*

DOI: http://dx.doi.org/10.1080/00958972.2016.1163547

Alkyl chain length effect on construction of copper(II) complexes with tridentate Schiff base ligand and DNA interaction

RASOUL VAFAZADEH*†, FARIBA JAFARI†, MOHAMMAD MEHDI HEIDARI‡ and ANTHONY C. WILLIS§

†Department of Chemistry, Yazd University, Yazd, Iran
‡Department of Biology, Yazd University, Yazd, Iran
§Research School of Chemistry, Australian National University, Canberra, ACT 2601, Australia

Two tridentate Schiff base ligands were synthesized by condensation of equimolar amounts of benzoylacetone and 2-amino-1-ethanol or 3-amino-1-propanol, H_2L^1 and H_2L^2, respectively. The reaction of the Schiff base ligands with $Cu(CH_3COO)_2$ in methanol leads to $(CuL^1)_4$, **1** and $(CuL^2)_2$, **2**. In the tetranuclear cubane species, the tridentate H_2L has both a chelating and a bridging mode, after double deprotonation of the enolic OH groups. The copper(II) centers are five-coordinate with a NO_4 donor set from the ligands. The coordination geometry around each copper ion is essentially square pyramidal with one nitrogen and two oxygens from one ligand and two oxygens of adjacent ligands from the next unit of the cubane. In dinuclear **2**, H_2L^2 has chelating and bridging modes after double deprotonation of the enolic OH groups. The dianionic form of the Schiff base coordinates forming a six-membered chelate ring with Cu(II). Two such monomeric CuL^2 entities are eventually linked through the alkoxo bridges to produce dinuclear **2**. The absorption spectra strongly suggest that **2** interacts with CT-DNA. Both **1** and **2** appear to be more efficient than the parent compound in DNA cleavage.

Keywords: Copper complex; Tridentate Schiff base; Tetranuclear; Dinuclear; DNA Interaction

*Correspondencing author. Email: rvafazadeh@yazd.ac.ir

1. Introduction

The design and synthesis of multinuclear transition metal complexes of Schiff bases have attracted research due to their relevance in bioinorganic chemistry [1-3], molecular magnetic materials [4-6], and the development of coordination chemistry [6-12]. There has been growing interest in using the self-assembly process in synthesis of multinuclear metal complexes. The most common ligands used for construction of polynuclear complexes by self-assembly are tridentate Schiff base ligands, which contain potentially bridging phenoxo or hydroxo oxygen and nitrogen donors [13-16].

Multinuclear copper complexes have attracted attention with interesting structures [17-20] and because copper is involved in many important biological activities [20-22]. Investigations of the interaction between multinuclear copper(II) complexes and DNA have attracted interest due to their importance in molecular biology [14, 23-29].

Herein, we report the synthesis, spectroscopic characterization, structural aspects and DNA interaction of one tetranuclear cubane $(CuL^1)_4$ and one dinuclear $(CuL^2)_2$ Schiff base complex. Two Schiff base ligands, H_2L^1 and H_2L^2 (with ONO donors), were obtained from 1:1 condensation of benzoylacetone and 2-amino-1-ethanol or 3-amino-1-propanol, respectively (scheme 1). The coordination sphere around copper(II) can be modified easily and led to a number of Cu(II) complexes with different nuclearity.

The syntheses of **1** and **2** were previously reported by the template method and their magnetic properties studied. Molecular weight measurements in chloroform on two different structures for these complexes have been suggested [30]. However, the synthesis of the free Schiff base ligands and crystallographic data of the complexes have not been reported.

2. Experimental

2.1. *Reagents*

All chemicals were used as supplied by Merck and Fluka without purification. Supercoiled pBR322 DNA was obtained from Sigma–Aldrich and stored at 4 °C. The tris(hydroxymethyl)aminomethane–HCl (Tris–HCl) buffer was prepared in doubly distilled water.

2.2. *Physical measurements*

Infrared spectra were taken with an Equinox 55 Bruker FT-IR spectrometer using KBr pellets from 400-4000 cm^{-1}. Absorption spectra of the ligands were determined in methanol and for **1** and **2** in DMF using a GBC UV-Visible Cintra 101 spectrophotometer with 1 cm quartz cells, from 200-800 nm at 25 °C. Elemental analyses (C, H and N) were performed using a CHNS-O 2400II PERKIN-ELMER elemental analyzer.

2.3. *DNA binding*

Interaction of the complexes with calf thymus CT-DNA was studied in Tris–HCl buffer (5.5 mM Tris–HCl, pH 7.2) containing 50 mM NaCl at room temperature. The solution was kept for over 24 h at 4 °C. The resulting, somewhat viscous, solution was clear and particle-free. CT-DNA in the buffer medium gave a ratio of UV absorbance at 260 and 280 nm of 1.8:1, indicating that the DNA was sufficiently free of protein [31]. The DNA concentration was measured from its absorption intensity at 260 nm using the molar absorption coefficient (ε) value of 6600 M^{-1} cm^{-1} as reported [32]. Stock solutions of complexes were freshly prepared by dissolving the complexes in DMF and diluting them with the buffer. The amount of DMF was kept at 10% (by volume) for each set of experiments and has no effect on the experimental results. Absorption spectral titrations were performed while maintaining a constant complex concentration and varying the nucleic acid concentration. This was achieved by dissolving an appropriate amount of the complexes (40 μM) and DNA stock solutions (0 - 54 μM) while maintaining the total volume constant (1 mL). Spectral bands were recorded after successive addition of CT-DNA. The Tris–HCl buffer was used as a blank to make preliminary adjustments. The intrinsic binding constant (K_b) of the complex to CT-DNA was determined from the spectral titration data using the following equation [33]:

$$[DNA]/(\varepsilon_a - \varepsilon_f) = [DNA]/(\varepsilon_b - \varepsilon_f) + 1/K_b(\varepsilon_b - \varepsilon_f) \qquad (1)$$

where [DNA] is the concentration of CT-DNA in base pairs and the apparent absorption coefficients ε_a, ε_f and ε_b correspond to A_{obs}/[DNA], the absorbance for the free-Cu(II) complex (unbound), and the absorbance for the fully-bound complex, respectively. A plot of $[DNA]/(\varepsilon_a - \varepsilon_f)$ versus [DNA] gave a slope $1/(\varepsilon_b - \varepsilon_f)$ and a intercept $1/K_b(\varepsilon_b - \varepsilon_f)$, so the value of K_b can be determined from the ratio of the slope to the intercept.

2.4. *DNA Cleavage*

Cleavage of plasmid DNA was monitored using agarose gel electrophoresis following the literature method [34-36]. Supercoiled pBR322 DNA (0.1 mg/mL, 1.5 μL) in Tris buffer (pH = 7.2, 5.0 mM Tris-HCl, 20 mM NaCl) with 50 mM NaCl was treated with varying concentrations of the copper(II) complexes (40-600 μM). The concentration of the complexes in the buffer corresponded to the quantity after the dilution of the complex stock to the 20 μL final volume using Tris buffer. The samples were incubated for 2 h at 37 °C, followed by addition of the loading buffer containing 12.5% bromophenol blue, 25% xylene cyanol, 1% tris, and the solution was finally loaded on agarose (1%) containing 10 mg/mL ethidium bromide (EB). The electrophoresis was carried out at 60 V for 3 h in Tris–acetate–EDTA. Afterwards, electrophoresis bands were visualized by UV light and photographed. The cleavage mechanism of pBR322 DNA was measured in the presence of H_2O_2 (oxidizing agent), DMSO (hydroxyl scavenger) and NaN_3 (singlet oxygen scavenger).

2.5. *X-ray Crystallography*

Diffraction images were measured at 200 K on a Nonius Kappa CCD diffractometer using Mo *K*α, graphite monochromator (λ = 0.71073 Å) and data extracted using the *DENZO*/*SCALEPACK* package [37]. The structures were solved by direct methods with SIR92 [38]. The structures were refined on F^2 by full matrix last-squares using the CRYSTALS program package [39]. Hydrogens were added at calculated positions and then refined with soft restraints on the bond lengths and angles to regularize their geometry. In **1** the hydrogens were then refined with riding constraints, whereas in **2** they were allowed to refine freely. Atomic coordinates, bond lengths and angles, and displacement parameters have been deposited at the Cambridge Crystallographic Data Centre. Crystallographic details for **1** and **2** are summarized in table 1.

2.6. *Syntheses*

2.6.1. Syntheses of H_2L^n. Two tridentate Schiff bases, H_2L^1 and H_2L^2, were synthesized by a general method using the condensation of an equimolar amount of benzoylacetone (5 mmol, 0.81 g) and the related amine (5 mmol), 2-amino-1-ethanol (0.3 mL) and 3-amino-1-propanol

(0.38 mL) in methanol (30 mL), respectively [40, 41]. Then the mixture was refluxed for 2 h, giving yellow micro crystals. The micro crystals were filtered off and re-crystallized in acetone/ethanol at room temperature.

H_2L^1: Yield: 0.89 g (87%). Anal. Calc. for $C_{12}H_{15}NO_2$ (205.26): C, 70.22; H, 7.37; N, 6.82%. Found: C, 70.51; H, 7.45; N, 6. 66%. IR (KBr, cm^{-1}): νOH 3357, νC=N 1602. Electronic spectra in CH_3OH λ_{max}(nm), (log ε): 237 (3.46), 342 (3.60).

H_2L^2: Yield: 0.89 g (81%). Anal. Calc. for $C_{13}H_{17}NO_2$ (219.28): C, 71.21; H, 7.81; N, 6.39%. Found: C, 71.48; H, 7.93; N, 6. 27%. IR (KBr, cm^{-1}): νOH 3379, νC=N 1602. Electronic spectra in CH_3OH λ_{max}(nm), (log ε): 243 (3.41), 343 (3.65).

2.6.2. Syntheses of $(CuL^1)_4$, 1 and $(CuL^2)_2$, 2. Complexes **1** and **2** were synthesized by a general method. Copper(II) acetate monohydrate (2 mmol 0.396 g) was slowly added to a methanol solution (30 mL) of the appropriate Schiff base (2 mmol, 0.41 g for **1** and 0.438 g for **2**). The resulting solution was stirred for 2 h at room temperature. The resulting dark-green precipitates were collected by filtration and dried in air.

$(CuL^1)_4$, 1. Dark-green needles suitable for X-ray analysis appeared upon slow evaporation from dichloromethane/methanol (1:1 v/v). Yield 72% (0.38 g). Anal. Calcd. for $(C_{12}H_{13}CuNO_2)_4$: C, 54.02; H, 4.91; N, 5.25. Found: C, 53.81; H, 4.79; N, 5.21. IR (KBr, cm^{-1}): $\nu_{C=N}$ = 1599, ν_{C-O} = 1331. Electronic spectra in DMF solvent λ_{max}, nm (log ε): 638 (1.40), 346 (3.64).

$(CuL^2)_2$, 2. Dark-green needle-shaped crystals appeared upon slow evaporation from dichloromethane/methanol (1:1 v/v). Yield 63% (0.35 g). Anal. Calcd. for $(C_{13}H_{15}CuNO_2)_2$: C, 55.60; H, 5.38; N, 4.99. Found: C, 55.88; H, 5.50; N, 5.07. IR (KBr, cm^{-1}): $\nu_{C=N}$ = 1590, ν_{C-O} = 1354. Electronic spectra in DMF solvent λ_{max}, nm (log ε): 584 (1.26), 345 (3.66).

3. Results and discussion

3.1. *Synthesis and characterization of the complexes*

Syntheses of **1** and **2** are schematically represented in scheme 1. The tridentate Schiff base ligands were obtained by condensation of benzoylacetone and amino-alcohol under reflux. The reaction of copper(II) acetate with an equimolar amount of H_2L^1 in methanol leads to tetranuclear **1**. When H_2L^2 was used for the synthesis, dinuclear **2** was formed.

The most significant IR bands for the ligands and complexes are given in the Experimental section. The IR spectra of the free Schiff bases show a band at 1602 cm^{-1}, assigned as νC=N. IR spectra of **1** and **2** show a decrease in νC=N in comparison with the free ligand, which indicates coordination of the imine nitrogen to copper [12, 41, 42]. The fairly broad band of medium intensity at 3357 and 3379 cm^{-1} corresponds to intramolecular hydrogen bonding in the free ligands, and this band disappears for the copper complexes. The lack of OH groups in the copper complexes indicates that the OH groups have been deprotonated and are coordinated to copper.

The electronic spectra of the copper complexes in DMF show a broad band at 638 (for **1**, log ε = 1.40) and 584 nm (for **2**, log ε = 1.26) and a sharper signal at 346 (for **1**, log ε = 3.64) and 345 nm (for **2**, log ε = 3.66), which arise from a spin-allowed d-d transition of the copper(II) ion (d^9 electronic configuration) and a charge transfer transition, respectively [43, 44].

3.2. *Crystal structure of 1*

The molecular structure of **1** is shown in figure 1. Selected bond lengths and angles as well as interatomic distances are summarized in table 2. Complex **1** crystallizes in trigonal space group *R*3.

In the copper complex, H_2L^1 has both chelating and bridging modes after double deprotonation of the enolic OH groups. The dianionic form of the Schiff base ligand coordinates to the metal center through the imine nitrogen and deprotonated alkoxo oxygens. By a self-assembly process, four monomeric CuL^1 entities are linked through alkoxo bridges to produce the tetranuclear cubane, **1**.

In **1**, the four alkoxo oxygens are located at the four corners of the cube and bridge the metal centers in a μ^3-fashion (O2: Cu1, Cu2, Cu3; O4: Cu2, Cu3, Cu4; O6: Cu1, Cu3, Cu4; O8: Cu1, Cu2, Cu4). Intracluster metal/metal separations of adjacent Cu···Cu distances are 3.105–3.399 Å, which are comparable with values of similar compounds [14, 45, 46]. The copper(II) centers are five-coordinate with a NO_4 donor set from the Schiff base ligands. The coordination geometry about each copper ion is a square pyramid with one nitrogen and two oxygens from the Schiff base ligand and two oxygens from the next unit of the cubane. According to the bond lengths between the copper and coordinating atoms (*i.e.*, four bonds with short bond distances, 1.908(3)–1.984(3) Å and bonds with long bond distances,

2.375(3)–2.622(3) Å) the basal planes for Cu1, Cu2, Cu3 and Cu4 are O1–N1–O2–O8, O2–N2–O3–O4, O4–N3–O5–O6 and O6–N4–O7–O8, respectively. The Cu ions in the tetranuclear species deviate from the corresponding mean planes by 0.067–0.144 Å, towards the apical ligand. The coordination spheres of the copper ions in the complex are best described as a distorted square pyramid according to the Addison parameter τ values of 0.05–0.19. The parameter τ is defined as $\tau = (\alpha-\beta)/60$, $\alpha>\beta$, where α and β are the largest angles, with $\tau = 1$ for a regular trigonal bipyramid and $\tau = 0$ for regular square pyramid [47].

The Cu–O and Cu–N bond lengths in the equatorial plane are 1.908–1.984 Å and 1.920–1.940 Å, respectively (table 2), which agree with similar compounds [12, 14, 41]. The apical oxygens show longer Cu–O(alkoxo) bond lengths than the equatorial oxygens [43, 48]. The elongation of the Cu–O axial bonds is due to a pseudo-Jahn–Teller distortion of the d^9 copper center. The lengths of the bonds between copper and the donor atoms are within the range of values normally found for such systems [14, 19, 49, 50].

The bridging bond angles of Cu–O(alkoxo)–Cu are 89.26–112.25° (table 2). It is evident from the different Cu–O body diagonal distances as well as from the unequal metal–metal distances (table 2) that the cubane core is not a regular one, but distorted. In tetranuclear **1**, the dihedral angles of adjacent phenyl rings are between 51–55°.

In the absence of suitably polar hydrogens there is no hydrogen bonding in the intra- and intermolecular interaction of the complex. However, the 3D lattice structure of **1** shows the presence of intermolecular non-covalent C–H ····· N=C and C–H(Ph) ····· C–H(Ph) interactions (figure 2).

3.3. *Crystal structure of 2*

The molecular structure of **2** is shown in figure 3. Selected bond lengths and angles as well as interatomic distances are summarized in table 2; **2** crystallizes in the monoclinic space group $P2_1/n$.

In **2**, similar to **1**, H_2L^2 is both chelating and bridging after double deprotonation of the enolic OH groups. The dianionic form of the ligand coordinates, forming six-membered chelate rings with Cu(II). Two such monomeric CuL^2 entities are eventually linked through the alkoxo bridges to produce the dinuclear **2**.

The dinuclear unit is formed by two Cu(II) ions labeled Cu1 and Cu1* (symmetry code: −x+1, −y+1, -z+1), bridged by the two μ_2−alkoxo oxygens of the Schiff base ligands. Coordination about each copper ion is square planar with one nitrogen and two oxygens from the Schiff base and one oxygen from the next unit of the dimer. The Cu–O, Cu–N, and two Cu–O_{bridge} bond distances are 1.9071(12), 1.9455(13), 1.9313(11) and 1.9197(11) Å, respectively, in agreement with those observed for similar compounds [12, 14, 49, 51]. As usually found in oxo-bridged Cu(II) complexes [12, 14, 52, 53], the Cu-O_{bridge} bond distances (1.9313(11) and 1.9197(11) Å) are slightly longer than the chelating Cu-O bond length (1.9071(12) Å) because of the weaker interaction of the binding alkoxo bridging with copper. The distance between the two Cu ions is 3.0341(4) Å, indicating the absence of any bond between the copper centers.

The angles involving the copper ions are different from 90° and 180°. The N–Cu–O *trans* angle is 172.87(5)°, the O–Cu–O *trans* angle is 167.26(5)° and the N–Cu–O *cis* angles are 95.03(5) and 96.56(5)° (table 2), indicating that there is distortion from ideal square planar geometry. The geometry of copper is best described as distorted square planar with τ_4 index 0.141. The τ parameter is $\tau_4 = [360° - (\alpha + \beta)]/141°$, where a and b are the largest angles around the central metal in the complex, $\tau_4 = 1$ for a regular tetrahedron and $\tau_4 = 0$ for a regular square planar [54]. The copper ions lie 0.043 Å above the NO_3 donor planes.

In **2** there are no intramolecular interactions. The crystal packing of the complex shows the presence of intermolecular non-covalent interactions between CH_2 units of the propylene to form a 2D planar network parallel to the *ab* plane (figure 4).

3.4. *DNA Binding studies*

UV–Visible spectroscopy was performed to study the interaction of the complexes with DNA keeping the complex concentration constant (40 μM) and varying the concentration of CT-DNA (0 – 54 μM). The change in absorbance values at 260 nm was used to evaluate the intrinsic binding constant K_b. The absorption spectra of **2** in the absence and presence of CT-DNA (at constant concentration of complex) are shown in figure 5. Hypochromicity of the DNA at 265 nm without a shift in band position is observed with the addition of CT-DNA.

The hypochromism (decrease of absorbance) indicated a strong interaction between the complexes and CT-DNA mainly through intercalative binding [55, 56]. The non-covalent

intercalative binding of the compound to the DNA helix can lead to large hypochromism due to the strong stacking interaction between the aromatic moiety of the complex and the base pairs of DNA [57, 58]. Complex **2** binds to DNA through intercalation and resulted in hypochromism due to the stacking effect of π electrons which leads to a decrease in the peak intensities in the UV spectra of complex [59, 60].

Analysis of the spectral data using Equation 1 in the presence of DNA (figure 5) gave a binding constant, K_b, of $(4.10\pm0.21)\times10^4\ M^{-1}$ for **2**. The K_b value is lower than that observed for classical intercalator EB (order of magnitude of $10^6\ M^{-1}$) [61], indicating that the compounds bind DNA with less affinity. However, the K_b value for **2** is comparable to that observed for copper(II) complexes, such as $[CuL1](ClO_4)_2$ (L1 = *N,N′*-bis-pyridin-2-ylmethyl-butane-1,4-diimine), $2.6\times10^4\ M^{-1}$ [62] and [Cu(bpy)2(pic)](pic) (pic = picrate), $2.6\times10^4\ M^{-1}$ [63] and higher than $[CuL_2]$ (HL = N-(3-hydroxybenzyl)-leucine acid), $1.55\times10^3\ M^{-1}$ [64], $[Cu(bpy)(Gly)Cl]\cdot2H_2O$, $1.84\times10^3\ M^{-1}$, $[Cu(dpa)(Gly)Cl]\cdot2H_2O$, $3.10\times10^3\ M^{-1}$ [65], [Cu(L)(bpy)Cl] (HL = (E)-3-(2-hydroxyphenylimino)-N-*o*-tolylbutanamide), $1.55\times10^3\ M^{-1}$ [66] $[Cu2(\mu\text{-}Cl)_2(O\text{-}2\text{-}alkoxyethylpyridine\text{-}2\text{-}carboximidate)_2Cl_2]$ complexes, where alkoxy = methoxy, ethoxy, and butoxy, 1.52×10^3, 5.59×10^3, and $6.36\times10^3\ M^{-1}$, respectively [67].

From the binding constant value, it was clear that **2** had good interaction with CT-DNA. However, **1** and free ligands H_2L^1 and H_2L^2 exhibited no significant DNA bonding.

3.5. *Supercoiled pBR322 plasmid DNA cleavage studies*

3.5.1. DNA cleavage with 1. DNA cleavage was analyzed by monitoring the conversion of supercoiled DNA (form I) to nicked circular DNA (form II) and linear DNA (form III). When circular plasmid DNA is subjected to electrophoresis, a relatively fast migration will be observed for the intact supercoil form (form I). If scission occurs on one strand (nicking), the supercoil will relax to generate a slower moving open circular form (form II). If both strands are cleaved, a linear form (form III) that migrates between form I and form II will be generated [43, 44]. At micro-molar concentrations, for 3 h incubation periods, in the absence of H_2O_2 (an oxidizing agent) **1** exhibited no significant nuclease activity (figure 6, lanes 2-5). However, **1** displays efficient cleavage of pBR322 circular plasmid DNA converting form I to form II and form III in the presence of hydrogen peroxide (figure 6, lane 6), indicating an oxidative cleavage process [36]. Control experiments using only H_2O_2 (200 μM), copper alone up to 200 μM and copper salt

in the presence of H_2O_2 did not show any significant DNA cleavage under similar experimental conditions (figure 7, lanes 2, 5 and 6, respectively). The reaction of pBR322 DNA with H_2L^1 (200 μM) in the absence of H_2O_2 did not exhibit any cleavage activity (figure 7, lane 3). H_2L^1, however, in the presence of H_2O_2 caused conversion of supercoiled structure into nicked circular (figure 7, lane 7). The control results suggest the complex to be more efficient than copper salt and ligand for the chemical nuclease activity.

To elucidate the cleavage mechanism of DNA, the cleavage was investigated in the presence of hydroxyl radical ($OH^{\bullet}$) scavenger (DMSO, 1.4 mM) and a singlet oxygen ($^1O_2$) quencher (NaN_3, 1 mM). The experiments reveal that NaN_3 and DMSO significantly inhibited the cleavage activity of Cu(II) complex (figure 6, lanes 7 and 8), indicating that singlet oxygen and hydroxyl radical play significant roles in the DNA cleavage reaction [68, 69]. The result suggests that **1** cleaves DNA via oxidative cleavage [35, 36].

3.5.2. DNA cleavage with 2. Complex **2** exhibited DNA cleavage activity even in the absence of an oxidant (figure 8, lanes 2-5). Control experiments using DNA alone (figure 8, lane 1) and only H_2L^2 (figure 7, lane 4) in the absence of **2** resulted in no significant cleavage of pBR322 circular plasmid DNA, even after long exposure times. From the observed results, it was concluded that **2** effectively cleaved the DNA as compared to control DNA and H_2L^2 alone. Upon increasing the concentration of **2** more cleavage activity was observed (figure 8, lanes 2-5). This shows that the concentration of optimal value led to extensive degradations, resulting in conversion of the supercoiled form (Form I) into a nicked circular form (Form II). The activity for DNA cleavage without an oxidant is often a hydrolytic rather than an oxidative mechanism [43].

Also, the nuclease activity of the complex was investigated in the presence of H_2O_2 as an oxidant and a hydroxyl radical scavenger, DMSO, and a singlet oxygen quencher, NaN_3. In the presence of H_2O_2, **2** shows higher activity and supercoiled DNA (Form I) is cleaved to form a mixture of Form II and Form III (figure 8, lane 6). The presence of DMSO did not significantly reduce the efficiency of DNA cleavage (figure 8, lane 7), ruling out the possibility of the involvement of diffusible hydroxyl radicals in the cleavage in the presence of H_2O_2 [39, 40]. However, the addition of the singlet quencher, NaN_3 significantly inhibited the cleavage activity

of **2** (figure 8, lane 9). The results suggest that singlet oxygen is responsible for the DNA cleavage in the presence of H_2O_2 [43].

4. Conclusion

We have synthesized a tetranuclear copper(II), **1**, and a dinuclear, **2**, complex with two tridentate Schiff base ligands. The complexes were structurally characterized by single crystal X-ray diffraction analysis. Complex **1** has a cubane Cu_4O_4 core in which copper and oxygen are present at alternative vertices. The coordination geometry about each copper ion is square pyramidal. Complex **2** contains a coplanar Cu_2O_2 core and the coordination geometry around the copper(II) is four-coordinate square planar. Complex **1** exhibits significant DNA cleavage activity in the presence of H_2O_2 as an oxidant. The binding of the complexes with CT-DNA was studied using UV-Vis spectroscopy. The absorption spectra indicate that **2** interacts with CT-DNA. Both complexes are more efficient than their parent compound in DNA cleavage.

Supplementary material

The deposition numbers of **1** and **2** are CCDC 1045677 and 1045678, respectively. These data can be obtained free of charge via www.ccdc.cam.ac.uk/data_request/cif, by emailing data-request@ccdc.cam.ac.uk, or by contacting the Cambridge Crystallographic Data Centre, 12 Union Road, Cambridge CB2 1EZ, UK; Fax +44 1223 336033.

Acknowledgements

The authors are grateful to the Yazd University and the Australian National University for partial support of this work.

References

[1] F. Yu, V. M. Cangelosi, M. L. Zastrow, M. Tegoni, J. S. Plegaria, A. G. Tebo, C. S. Mocny, L. Ruckthong, H. Qayyum, V. L. Pecoraro, *Chem. Rev.,* **114**, 3495 (2014).

[2] H. Wu, G. Pan, Y. Bai, H. Wang, J. Kong, F. Shi, Y. Zhang, X. Wang, *J. Coord. Chem.,* **66,** 2634 (2013).

[3] S. Mukhopadhyay, S. K. Mandal, S. Bhaduri, W. H. Armstrong. *Chem. Rev*. **104,** 3981 (2004).

[4] M. Nandy, S. Shit, P. Dhal, C. Rizzoli, C. J. Gómez–García, S. Mitra. *J. Coord. Chem.*, **68**, 916 (2015).

[5] F. Zeng, J. Ni, C. Ding, Y. Xie. *J. Coord. Chem.*, **65**, 2247 (2012).

[6] B. Shaabani, A.A. Khandar, M. Dusek, M. Pojarova, F. Mahmoudi, A. Feher, M. Kajňaková. *J. Coord. Chem.*, **66**, 748 (2013).

[7] C.J. Lin, J.L. Qi, Y.Q. Zheng, J.L. Lin. *J. Coord. Chem.*, **66**, 3877 (2013).

[8] T.R. Cook, Y.-R. Zheng, P.J. Stang. *Chem. Rev.*, **113**, 734 (2013).

[9] S. Shit, U. Yadava, D. Saha, R. Fröhlich. *J. Coord. Chem.*, **66**, 66 (2013).

[10] R. Vafazadeh, B. Khaledi, A.C. Willis, M. Namazian. *Polyhedron*, **30**, 1815 (2011).

[11] R. Vafazadeh, B. Khaledi, A.C. Willis. *Acta Chim. Slov.*, **59**, 954 (2012).

[12] R. Vafazadeh, R. Esteghamat-Panah, A.C. Willis, A.F. Hill. *Polyhedron*, **48**, 51 (2012).

[13] C.-H. Zhang, Y.-G. Chen. *J. Cluster Sci.*, **25**, 435 (2014).

[14] R. Vafazadeh, A.C. Willis. *J. Coord. Chem.*, **68**, 2240 (2015).

[15] A.P. Neves, K.C.B. Maia, M.D. Vargas, L.C. Visentin, A. Casellato, M.A. Novak, A.S. Mangrich. *Polyhedron*, **29**, 2884 (2010).

[16] D. Venegas-Yazigi, D. Aravena, E. Spodine, E. Ruiz, S. Alvarez. *Coord. Chem. Rev.*, **254**, 2086 (2010).

[17] P.K. Bhaumik, K. Harms, S. Chattopadhyay. *Polyhedron*, **67**, 181 (2014).

[18] R.C. Santra, K. Sengupta, R. Dey, T. Shireen, P. Das, P.S. Guin, K. Mukhopadhyay, S. Das. *J. Coord. Chem.*, **67**, 265 (2014).

[19] P. Bhowmik, N. Aliaga-Alcalde, V. Gómez, M. Corbella, S. Chattopadhyay. *Polyhedron*, **49**, 269 (2013).

[20] W. Xu, H.L. Zhu, J.L. Lin, Y.Q. Zheng. *J. Coord. Chem.*, **66**, 171 (2013).

[21] C. Demetgül, M. Karakaplan, S. Serın, M. Diğrak. *J. Coord. Chem.*, **62**, 3544 (2009).

[22] E.I. Solomon, D.E. Heppner, E.M. Johnston, J.W. Ginsbach, J. Cirera, M. Qayyum, M.T. Kieber-Emmons, C.H. Kjaergaard, R.G. Hadt, L. Tian. *Chem. Rev.*, **114**, 3659 (2014).

[23] M. Iqbal, S. Ali, Z.U. Rehman, N. Muhammad, M. Sohail, V. Pandarinathan. *J. Coord. Chem.*, **67**, 1731 (2014).

[24] R. Vafazadeh, N. Hasanzade, M.M. Heidari, A.C. Willis. *Acta Chim. Slov.*, **62**, 122 (2015).

[25] H.H. Lu, Y.T. Li, Z.Y. Wu, K. Zheng, C.W. Yan. *J. Coord. Chem.*, **64**, 1360 (2011).

[26] Y. Mei, J.J. Zhou, H. Zhou, Z.Q. Pan. *J. Coord. Chem.*, **65**, 643 (2012).

[27] R.K.B. Devi, S.P. Devi, R.K.B. Singh, R.K.H. Singh, T. Swu, W.R. Devi, CH.B. Singh. *J. Coord. Chem.*, **67**, 891 (2014).

[28] M. Iqbal, S. Ali, Z.-U.r Rehman, N. Muhammad, M. Sohail, V. Pandarinathan. *J. Coord. Chem.*, **67**, 1731 (2014).

[29] M. Nandy, D.L. Hughes, G.M. Rosair, R.K.B. Singh, S. Mitra. *J. Coord. Chem.*, **67**, 3335 (2014).

[30] K. Hines, L.J. Theriot. *Synth. React. Inorg. Met.-Org. Chem.*, **21**, 89 (1991).

[31] J. Marmur, P. Doty. *J. Mol. Biol.*, **3**, 585 (1961).

[32] M.E. Reichmann, S.A. Rice, C.A. Thomas, P. Poty. *J. Am. Chem. Soc.*, **76**, 3047 (1954).

[33] A. Wolf, G.H. Shimer, T. Meehan. *Biochemistry*, **26**, 6392 (1987).

[34] L. Subha, C. Balakrishnan, S. Thalamuthu, M.A. Neelakantan. *J. Coord. Chem.*, **68**, 1021 (2015).

[35] X.-T. Zhang, Z.-Y. Ma, C. Zhao, C.-Z. Xie, J.-Y. Xu. *J. Coord. Chem.*, **68**, 2307 (2015).

[36] Q.R. Cheng, F.Q. Zhang, H. Zhou, Z.Q. Pan, G.Y. Liao. *J. Coord. Chem.*, **68**, 1997 (2015).

[37] Z. Otwinowski, W. Minor, *Methods in Enzymology*, C.W. Carter Jr., R.M.W. Sweet (Eds.), Vol. 276, p. 307, Academic Press, New York (1997).

[38] A. Altomare, G. Cascarano, G. Giacovazzo, A. Guagliardi, M.C. Burla, G. Polidori, M. Camalli. *J. Appl. Cryst.*, **27**, 435 (1994).

[39] P.W. Betteridge, J.R. Carruthers, R.I. Cooper, K. Prout, D.J. Watkin. *J. Appl. Cryst.*, **36**, 1487 (2003).

[40] R. Vafazadeh, A. Gorji, S. Ansari, A.C. Willis. *Acta Chim. Slov.*, **59**, 897 (2012).

[41] R. Vafazadeh, M. Alinaghi, A.C. Willis, A. Benvidi. *Acta Chim. Slov.*, **61**, 121 (2014).

[42] A.A. Nejo, G.A. Kolawole, A.O. Nejo. *J. Coord. Chem.*, **63**, 4398 (2010).

[43] M.-L. Liu, M. Jiang, K. Zheng, Y.-T. Li, Z.-Y. Wu, C.-W. Yan. *J. Coord. Chem.*, **67**, 630 (2014).

[44] R. Benramdane, F. Benghanem, A. Ourari, S. Keraghel, G. Bouet. *J. Coord. Chem.*, **68**, 560 (2015).

[45] V. Chandrasekhar, L. Nagarajan, R. Clerac, S. Ghosh, S. Verma. *Inorg. Chem.*, **47**, 1067 (2008).

[46] S. Thakurta, P. Roy, R.J. Butcher, M.S. El Fallah, J. Tercero, E. Garribba, S. Mitra. *Eur. J. Inorg. Chem.*, 4385 (2009).

[47] A.W. Addison, N. Rao, J. Reedijk, J.V. Rijn, G.C. Verschoor. *J. Chem. Soc., Dalton Trans.*, 1349 (1984).

[48] J. Lakshmipraba, S. Arunachalam, R. Vijay Solomon, P. Venuvanalingam. *J. Coord. Chem.*, **68**, 1374 (2015).

[49] J. Chakraborty, S. Thakurta, G. Pilet, D. Luneau, S. Mitra. *Polyhedron*, **28**, 819 (2009).

[50] P. Mukherjee, M.G.B. Drew, M. Estrader, C. Diaz, A. Ghosh. *Inorg. Chim. Acta*, **361**, 161 (2008).

[51] X.-J. Li, K. Zheng, Y.-T. Li, C.-W. Yan, Z.-Y. Wu, S.-Y. Xuan. *J. Coord. Chem.*, **68**, 928 (2015).

[52] A. Biswas, M.G.B. Drew, J. Ribas, C. Diaz, A. Ghosh. *Eur. J. Inorg. Chem.*, 2405 (2011).

[53] P. Zabierowski, J. Szklarzewicz, K. Kurpiewska, K. Lewinski, W. Nitek. *Polyhedron*, **49**, 74 (2013).

[54] P. Seth, S. Ghosh, A. Figuerola, A. Ghosh. *Dalton Trans.*, **43**, 990 (2014).

[55] J.K. Barton, A.T. Danishefsky, J.M. Goldberg. *J. Am. Chem. Soc.*, **106**, 2172 (1984).

[56] Y. An, S.D. Liu, S.Y. Deng, L.N. Ji, Z.W. Mao. *J. Inorg. Biochem.*, **100**, 1586 (2006).

[57] J. Chen, X. Wang, Y. Shao, J. Zhu, Y. Zhu, Y. Li, Q. Xu, Z. Guo. *Inorg. Chem.*, **46**, 3306 (2007).

[58] J.K. Barton, A.T. Danishefsky, J.M. Goldberg. *J. Am. Chem. Soc.*, **106**, 2172 (1984).

[59] K. Abdi, H. Hadadzadeh, M. Weil, M. Salimi. *Polyhedron*, **31**, 638 (2012).

[60] H. Hadadzadeha, M. Salimi, M. Weil, Z. Jannesari, F. Darabi, K. Abdi, A.D. Khalaji, S. Sardari, R. Ahangari. *J. Mol. Struct.*, **1022**, 172 (2012).

[61] X. Fan, J. Dong, R. Min, Y. Chen, X. Yi, J. Zhou, S. Zhang. *J. Coord. Chem.*, **66**, 4268 (2013).

[62] V. Uma, A. Castineiras, B.U. Nair. *Polyhedron*, **26**, 3008 (2007).

[63] M.-L. Liu, M. Jiang, K. Zheng, Y.-T. Li, Z.-Y. Wu, C.-W. Yan. *J. Coord. Chem.*, **67**, 3335 (2014).

[64] V. Uma, M. Kanthimathi, J. Subramanian, B.U. Nair. *Biochim. Biophys. Acta*, **1760**, 814 (2006).

[65] M.S. Mohamed, A.A. Shoukry, A.G. Ali. *Spectrochim. Acta, Part A*, **86**, 562 (2012).

[66] K. Pothiraj, T. Baskaran, N. Raman. *J. Coord. Chem.*, **65**, 2110 (2012).

[67] R.K.B. Devi, S.P. Devi, R.K.B. Singh, R.K.H. Singh, T. Swu, W.R. Devi, C.B. Singh. *J. Coord. Chem.*, **67**, 891 (2014).

[68] Z. Li-Hua, W. Wei-Na, W. Yuan, S. Guang. *J. Coord. Chem.*, **66**, 227 (2013).

[69] U. Chaveerach, A. Meenongwa, Y. Trongpanich, C. Soikumc, P. Chaveerach. *Polyhedron*, **29**, 731 (2010).

Figure captions

Figure 1. The molecular structure of tetranuclear **1** with labeling of selected atoms.

Figure 2. Packing diagram of tetranuclear cubane, **1**.

Figure 3. The molecular structure of dinuclear **2** with labeling of selected atoms.

Figure 4. Fragment of the molecular packing for **2** along the *c* axis.

Figure 5. Absorption spectra of **1** (40 μM) in Tris–HCl buffer (pH = 7.2) with increase in molar ratio of DNA to complex (0–54 μM). Arrow shows the absorbance change upon increase of DNA concentration. The inset shows plot of $[DNA]/(\varepsilon_a - \varepsilon_f)$ vs. [DNA] for titration of CT–DNA with the complex.

Figure 6. Agarose gel electrophoresis diagram showing the chemical nuclease activity of **1** using supercoiled pBR322 plasmid DNA (0.1 mg/mL, 1.5 μL): lane 1, DNA control; lane 2, DNA + **1** (50 μM); lane 3, DNA + **1** (100 μM); lane 4, DNA + **1** (300 μM); lane 5, DNA + **1** (600 μM); lane 6, DNA + **1** (300 μM) + H_2O_2 (3.2 mM); lane 7, DNA + **1** (300 μM) + H_2O_2 (3.2 mM) + DMSO (1.4 mM); lane 8, DNA + **1** (300 μM) + H_2O_2 (3.2 mM) + NaN_3 (1 mM).

Figure 7. Agarose gel electrophoresis diagram showing the chemical nuclease activity of the control experiments using Supercoiled pBR322 plasmid DNA (0.1 mg/mL, 1.5 μL): lane 1, alone DNA control; lane 2, DNA + copper salt (200 μM); lane 3, DNA + H_2L^1 (200 μM); lane 4, DNA + H_2L^2 (200 μM); lane 5, DNA + H_2O_2 (3.2 mM); lane 6, DNA + + copper salt (200 μM) + H_2O_2 (3.2 mM); lane 7, DNA + H_2L^1 (200 μM) + H_2O_2 (3.2 mM); lane 8, DNA + H_2L^2 (200 μM) + H_2O_2 (3.2 mM).

Figure 8. Agarose gel electrophoresis diagram showing the chemical nuclease activity of **2** using supercoiled pBR322 plasmid DNA (0.1 mg/mL, 1.5 μL): lane 1, DNA control; lane 2, DNA + **2** (40 μM); lane 3, DNA + **2** (100 μM); lane 4, DNA + **2** (200 μM); lane 5, DNA + **2** (400 μM); lane 6, DNA + **2** (200 μM) + H_2O_2 (3.2 mM); lane 7, DNA + **2** (200 μM) + H_2O_2 (3.2 mM) + DMSO (1.4 mM); lane 8, DNA + H_2O_2 (3.2 mM); lane 9, DNA + **2** (200 μM) + H_2O_2 (3.2 mM) + NaN_3 (1 mM).

Table 1. Crystallographic data of **1** and **2**.

Compound	**1**	**2**
Chemical formula	$C_{48}H_{52}Cu_4N_4O_8$	$C_{26}H_{30}Cu_2N_2O_4$
Formula weight	1067.15	561.62
Temperature (K)	200	200
Space group	Trigonal, *R*3, *Z*=9	Monoclinic, $P2_1/n$, *Z*=2
Unit cell dimensions		
a (Å)	30.1694(3)	7.3562(1)
b (Å)	30.1694(3)	9.9489(1)
c (Å)	17.7291(1)	16.2141(3)
α (°)	90	90
β (°)	90	96.5724(9)
γ (°)	120	90
V (Å^3)	11610.21(18)	1178.85(3)
F(000)	4932	580
D_{Calc} (g cm^{-3})	1.374	1.582
Crystal size (mm)	0.47×0.06×0.01	0.35×0.18×0.12
μ (mm^{-1})	1.68	1.84
θ range (°)	2.7 - 27.5	2.9 - 30.1
Limiting indices	$-39 \le h \le 39$	$-10 \le h \le 10$
	$-33 \le k \le 33$	$-13 \le k \le 14$
	$-18 \le l \le 19$	$-22 \le l \le 22$
No. independent reflns.	11670	3435
No. reflns. $F^2 > 2\sigma(F^2)$	9829	3012
No. parameters	578	199
$R[F^2 > 2\sigma(F^2)]$	0.040	0.031
$wR(F^2)$ (all data)	0.112*	0.083**
S (all data)	0.94	0.99

* w = [weight]*[1-(deltaF/6*sigmaF)^2]^2 where [weight] = 1/[A_0*T_0(x) + A_1*T_1(x) +⋯+ A_{n-1}*T_{n-1}(x)], where A_i = Chebychev coefficients 12.6, 18.1, 9.39, 2.80 and x = F/F_{max}

**w = 1/[$\sigma^2(F^2)$ + (0.05P)^2 + 0.73P], where P = (max(F_o^2,0) + 2F_c^2)/3

Table 2. Selected bond lengths (Å) and angles (°) in **1** and **2**[a].

Complex **1**			
Cu1–O1	1.908(3)	O1–Cu1–O2	179.05(16)
Cu1–O2	1.963(3)	O8–Cu1–N1	167.92(18)
Cu1–O6	2.375(3)	O6–Cu1–N1	113.33(16)
Cu1–O8	1.956(3)	O2–Cu1–O6	83.71(13)
Cu1–N1	1.934(4)	O3–Cu2–O4	173.36(14)
Cu2–O2	1.964(3)	O2–Cu2–N2	168.52(15)
Cu2–O3	1.917(3)	O8–Cu2–N2	109.13(14)
Cu2–O4	1.972(3)	O3–Cu2–O8	98.43(13)
Cu2–O8	2.387(3)	O5–Cu3–O6	173.50(16)
Cu2–N2	1.940(4)	O4–Cu3–N3	170.33(15)
Cu3–O2	2.622(4)	O2–Cu3–N3	108.15(14)
Cu3–O4	1.984(3)	O4–Cu3–O5	94.11(14)
Cu3–O5	1.908(3)	O7–Cu4–O8	174.98(14)
Cu3–O6	1.960(3)	O6–Cu4–N4	163.41(15)
Cu3–N3	1.923(4)	O4–Cu4–N4	117.77(15)
Cu4–O4	2.416(3)	O6–Cu4–O7	96.40(14)
Cu4–O6	1.966(3)	Cu3–O2–Cu2	89.26(12)
Cu4–O7	1.918(3)	Cu2–O2–Cu1	104.55(15)
Cu4–O8	1.961(3)	Cu4–O4–Cu3	91.36(12)
Cu4–N4	1.920(4)	Cu2–O4–Cu3	112.25(16)
Cu1···Cu2	3.016(1)	Cu1–O6–Cu4	92.18(12)
Cu1···Cu3	3.399(1)	Cu1–O6–Cu3	102.85(14)
Complex **2**			
Cu1–O2*	1.9313(11)	O2*–Cu1–O1	92.01(5)
Cu1–O1	1.9071(12)	O2*–Cu1–O9	76.03(5)
Cu1–O2	1.9197(11)	O1–Cu1–O2	167.26(5)
Cu1–N1	1.9455(13)	O2*–Cu1–N1	172.87(5)
O1–C7	1.297(2)	O1–Cu1–N1	95.03(5)
O2–C13	1.4108(19)	O2–Cu1–N1	96.86(5)
Cu1···Cu1*	3.0341(4)	Cu1–O2*–Cu1*–O2	0.0
		Cu1–O2*–Cu1*–N1*	179.45(6)

[a] symmetry code: –x+1, –y+1, –z+1

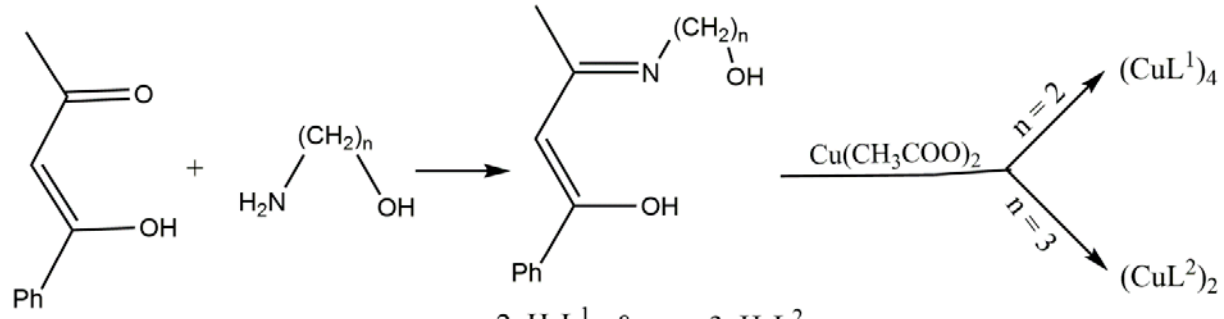

n = 2, H_2L^1 & n = 3, H_2L^2